nature structural & molecular biology

Insights into dynein motor domain function from a 3.3-Å crystal structure

Helgo Schmidt, Emma S Gleave & Andrew P Carter

Dyneins power the beating of cilia and flagella, transport various intracellular cargos and are necessary for mitosis. All dyneins have a ~300-kDa motor domain consisting of a ring of six AAA+ domains. ATP hydrolysis in the AAA+ ring drives the cyclic relocation of a motile element, the linker domain, to generate the force necessary for movement. How the linker interacts with the ring during the ATP hydrolysis cycle is not known. Here we present a 3.3-Å crystal structure of the motor domain of *Saccharomyces cerevisiae* cytoplasmic dynein, crystallized in the absence of nucleotides. The linker is docked to a conserved site on AAA5, which is confirmed by mutagenesis as functionally necessary. Nucleotide soaking experiments show that the main ATP hydrolysis site in dynein (AAA1) is in a low-nucleotide affinity conformation and reveal the nucleotide interactions of the other three sites (AAA2, AAA3 and AAA4).

Dyneins are a family of motor proteins that use the energy of ATP hydrolysis to move along microtubules. Axonemal dyneins power the beating of cilia and flagella. Intraflagellar transport (IFT) dynein is necessary for axoneme biogenesis. Cytoplasmic dynein is involved with a wide array of cellular processes, from regulating the spindle assembly checkpoint and transport of organelles to localization of RNAs and gathering up of misfolded proteins[1]. Dyneins are also associated with a number of disease processes, including viral transport[2], failure of neuron migration in lissencephaly[1], and axonemal disorders such as primary ciliary dyskinesia[3] and neurodegeneration[4].

All dyneins share a conserved motor domain, whose overall organization has been revealed by EM[5,6] and, more recently, low-resolution X-ray crystallography studies[7,8] (**Fig. 1a**). The motor domain consists of a ring of six ATPases associated with diverse cellular activities (AAA+) domains[9]. Each AAA+ domain can be subdivided into an αβ or 'large' (AAAL) subdomain and a five-helix bundle or 'small' subdomain (AAAS). All six AAA+ domains (AAA1–AAA6) are linked together in one polypeptide (**Fig. 1a**). AAA1 is the main hydrolysis site of the dynein motor domain[10–12], but the role of nucleotide binding at three other sites (AAA2–AAA4) is unclear[11–13]. In addition to the AAA+ ring, other structures allow dynein to act as a motor. The microtubule binding domain (MTBD) is at the end of a 15-nm stalk made up of an antiparallel coiled coil emanating from AAA4S. The base of the stalk is reinforced by a coiled coil extension from AAA5S called the buttress (or strut[8]), which is likely to couple ATP binding to altered microtubule affinities of the MTBD[7]. To move the motor along microtubules, force is generated by ATP hydrolysis at AAA1, driving the cyclic relocation of a motile element called the linker. Upon ATP binding, the linker exits the ring closer to AAA2 (pre–power stroke position), whereas in the absence of nucleotide or in the presence of ADP, it moves to exit the ring close to the base of the stalk (post–power stroke position)[5,6,11].

Despite recent advances in our knowledge of dynein structure[7,8], little is known about how ATP hydrolysis is coupled to the generation of force in dynein. Are there defined docking sites for the linker in the pre- and post–power stroke conformations, and if so, what do they look like? Is the linker in the same position in the nucleotide-free (apo) and ADP-bound forms of the motor, and how is ATP turnover at AAA1 connected to changes in the position of the linker? Also, compared to AAA1, the roles of the other ATPase domains (AAA2–AAA4) are less clear, as there is contradictory evidence on whether one[13–15] or two[16,17] ATPs are hydrolyzed per dynein step. In addition, mutations in these sites reduce but do not abolish dynein motility[11–13], raising the question of what function they might have during the dynein mechanochemical cycle. Here we present the high-resolution X-ray crystal structure of a dynein motor domain and provide insights into these questions.

RESULTS

Structure determination

To solve the dynein motor domain at 3.3 Å, we used an under-oil batch crystallization method to improve the diffraction and reproducibility of crystals grown using a glutathione *S*-transferase (GST)-dimerized dynein motor domain construct with a truncated stalk (GST-Dyn1-314kD$_{\Delta 3039\text{-}3291}$)[7]. The related construct (GST-Dyn1-314kD), containing a full-length stalk, walks normally along the microtubule, with velocities comparable to those of wild-type yeast dynein[14]. The truncated-stalk version shows ATPase activity (22.1 μM P_i s^{-1} μM^{-1} dimer) and undergoes ATP-dependent vanadate-mediated UV cleavage[10] (**Supplementary Fig. 1**) in AAA1, showing that the main dynein site of hydrolysis responds to nucleotide. These experiments

Medical Research Council Laboratory of Molecular Biology, Cambridge, UK. Correspondence should be addressed to A.P.C. (cartera@mrc-lmb.cam.ac.uk).

Received 1 February; accepted 28 February; published online 14 March 2012; doi:10.1038/nsmb.2272

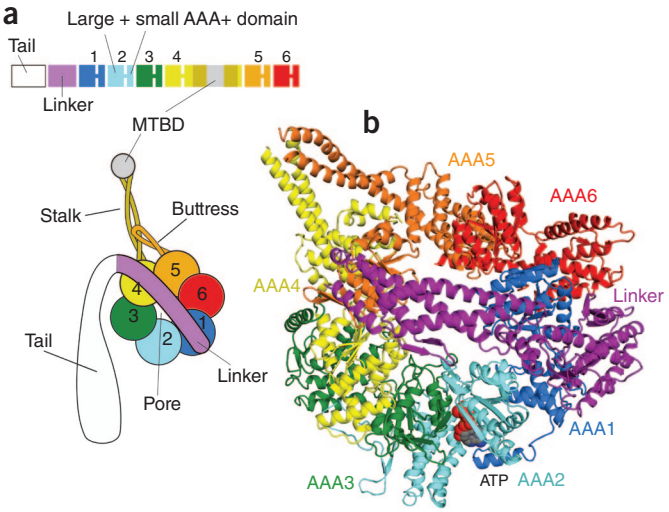

Figure 1 Overview of the dynein motor domain. (**a**) Cartoon of the domain organization of the dynein motor, showing the ring of six AAA+ domains. The stalk with the MTBD at its tip emerges from AAA4 and is contacted by the buttress from AAA5. The linker spans across the AAA+ ring and connects into the N-terminal tail. (**b**) Top view of a single dynein motor domain, crystallized in the absence of added nucleotide (LuAc dataset), showing AAA+ domains colored as in **a**. ATP is firmly bound at the AAA2 nucleotide binding site (AAA2-AAA3 cleft).

indicate that the construct is an active ATPase, and they can thus provide important insights into the dynein ATPase cycle.

We obtained phases by collecting SAD datasets from LuAc and Na_2WO_4 derivatives. Several rounds of multicrystal averaging, phase extension and model building were used to produce maps of sufficient quality to build a model that could be refined against a non–nucleotide-soaked dataset (LuAc) and against datasets from crystals soaked with different nucleotides (**Table 1**). The finished structure (**Fig. 1b**) reveals a wealth of new data compared to a previous low-resolution structure (PDB 3QMZ)[7]. It is at a high enough resolution to build side chains and nucleotides (**Supplementary Fig. 2a–f**) and previously unseen loop regions, including the long connector peptides that link AAA+ domains together (**Supplementary Fig. 2g,h**).

Interaction of the linker with the AAA+ ring

The linker is divided into four subdomains (**Fig. 2a**). The N-terminal subdomain 1 contacts AAA5L, and subdomain 2 spans over the pore of the AAA+ ring. The C-terminal subdomains 3 and 4 interact with AAA1L through extensive contacts, suggesting the linker is tightly connected to the AAA+ ring at this point. The middle of the linker consists of the junction between subdomains 2 and 3. Notably, unlike the rest of the linker, where there are multiple interactions between subdomains, this hinge-like junction appears to form a deep cleft (**Fig. 2b**) with only a single helix at its base.

The contact site between subdomain 1 and AAA5L consists of a hydrophobic pocket on subdomain 1 that accommodates a phenylalanine (Phe3446) on AAA5L, as well as a number of surrounding electrostatic interactions (**Fig. 2c**). To directly test the functional relevance of this site, we mutated Phe3446 and the surrounding residues in the background of a GST-dimerized, truncated dynein motor construct (GST-Dyn1-331kD), which moves similarly to full-length native dynein[14]. The mutations resulted in severe motility defects (**Fig. 2d**), abnormally strong microtubule binding states and impaired ATPase activities (**Supplementary Fig. 3a,b**). These data, together with the high conservation of

Table 1 Data collection, phasing and refinement statistics

	ATP	ADP[a]	AMP-PNP	LuAc[b]	Na_2WO_4	Native
Data collection						
Space group	$P2_1$	$P2_1$	$P2_1$	$P2_1$	$P2_1$	$P2_1$
Cell dimensions						
a, *b*, *c* (Å)	175.3, 117.9,202.8	174.9, 119.2, 194.0	175.6, 118.1, 201.0	175.8, 118.2,202.7	175.9, 118.1, 199.8	174.9, 118.3, 204.0
α, β, γ (°)	90, 90.2, 90	90.0, 90.2, 90.0	90.0, 90.3, 90.0	90.0, 90.9, 90.0	90.0, 91.1, 90.0	90.0, 90.6, 90.0
Resolution (Å)	87.7 (3.3)	49.2 (3.4)	80.3 (3.6)	49.1 (3.7)	81.1 (3.9)	66.2 (3.5)
R_{sym}	8.6 (101.5)	12.1 (187.5)	10.2 (68.8)	15.4 (175.6)	10.8 (107.7)	8.4 (82.1)
$I / \sigma I$	10.1 (1.7)	19.4 (2.6)	7.6 (2.2)	9.4 (2.0)	9.0 (2.1)	6.5 (1.4)
Completeness (%)	96.1 (86.5)	99.9 (100.0)	99.2 (97.5)	99.9 (99.7)	99.9 (99.9)	98.1 (94.7)
Redundancy	5.5 (5.2)	21.8 (21.8)	5.1 (4.6)	9.9 (8.1)	7.4 (7.5)	3.2 (3.0)
Refinement						
Resolution (Å)	50.0–3.3	49.3–3.4	50.0–3.6	49.1–3.7		
No. reflections	113,780	104,357	90,155	84,466		
R_{work} / R_{free}	23.9/30.5	24.1/30.3	24.1/30.2	23.1/28.9		
No. atoms	41,628	41,679	41,642	41,590		
Protein	41,490	41,497	41,469	41,496		
Ligand/ion	138	182	146	94		
B-factors						
Protein	164.1	184.7	176.5	192.2		
Ligand/ion	119.2	154.8	145.7	159.5		
R.m.s. deviations						
Bond lengths (Å)	0.011	0.010	0.010	0.010		
Bond angles (°)	1.61	1.56	1.49	1.51		

Values in parentheses are for highest-resolution shell.
[a]Four crystals; [b]Two crystals.

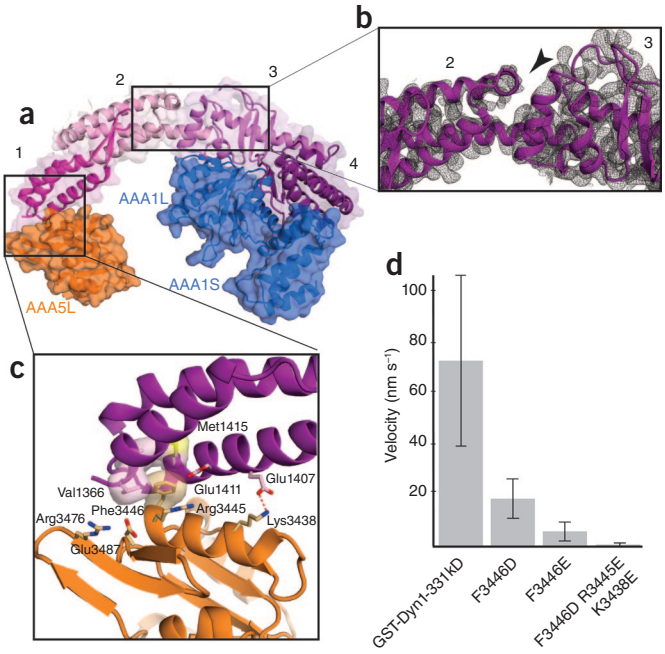

Figure 2 Interaction of the linker with the AAA+ ring. (**a**) The four subdomains of the linker are colored different shades of purple and are numbered. Subdomain 1 interacts with AAA5, and subdomains 3 and 4 interact with AAA1. (**b**) Cleft in the linker domain. The black arrowhead points to the cleft separating the linker into two halves, between subdomains 2 and 3. The map-sharpened $2F_o - F_c$ electron density of the ATP-soaked crystal structure is contoured at 1σ. (**c**) Interaction site between the linker and AAA5L. The highly conserved Phe3446 of AAA5 contacts hydrophobic residues of the linker, and Arg3445 and Lys3438 mediate electrostatic interactions between AAA5L and the linker. (**d**) Velocity of GST-dimerized truncated dynein motors in a single-molecule assay. Results from assays of GST-Dyn1-331kD (wild type) and mutations are shown. For the wild type, 600 measurements were carried out, and 400 measurements were done for each of the mutants; error bars represent the s.d. More severe mutation of the linker-AAA5 interface leads to a greater reduction in velocity.

the mutated residues among cytoplasmic dyneins (**Fig. 3a–c**), are consistent with the notion that linker binding to the AAA5 site is required for the dynein ATP hydrolysis cycle.

In addition to the AAA5L site, patches enriched in conserved residues also exist at AAA1L and two β-hairpins of AAA2 (**Fig. 3a**,**b**,**d**,**e**). The two β-hairpins are close to a conserved patch on the linker found at the cleft between subdomains 2 and 3 (arrowheads in **Figs. 2c** and **3d**,**e**). The AAA2 site forms the only highly conserved patch on the AAA+ ring not contacting the linker (**Fig. 3a**,**b**), which implies it might do so at some point of the mechanochemical cycle and that the linker therefore switches between two alternate ring docking sites during the power stroke.

Nucleotide binding to the AAA+ ring

The nucleotide binding sites sit between neighboring AAA+ domains. The first large domain contributes the Walker A motif (P-loop), which binds phosphate groups; the Walker B motif, which contains a magnesium-coordinating aspartate followed by the catalytic glutamate residue; and the sensor 1 hydrophilic residue, which also contributes to

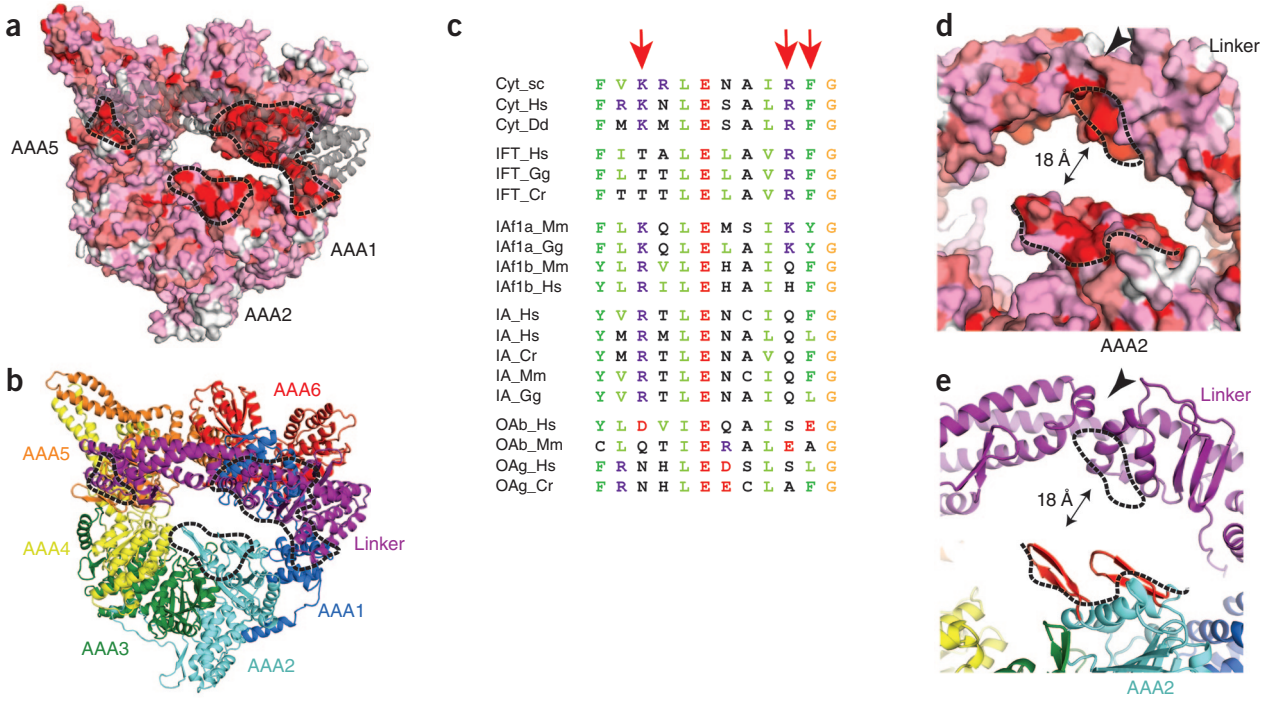

Figure 3 Conservation plots of the dynein motor domain. (**a**) Surface conservation plot of the linker proximal face of the AAA+ ring (white, not conserved among cytoplasmic dyneins; red, strictly conserved). The linker is shown in a gray transparent cartoon representation. The black dotted lines indicate surface patches that are enriched in strictly conserved amino acid residues (the AAA5 site corresponds to **Fig. 2c**). (**b**) Color-coded cartoon representation of the plot shown in **a**. (**c**) Sequence alignments of the AAA5-linker interaction site shown in **Figure 2c**. Cyt, cytoplasmic dynein; IAf, heterodimeric inner arm dynein; IA, monomeric inner arm dynein; OA, outer arm dynein. The red arrows point to Lys3438, Arg3445 and Phe3446. Cr, *Chlamydomonas reinhardtii*; Dd, *D. discoideum*; Gg, *Gallus gallus*; Hs, *Homo sapiens*; Mm, *Mus musculus*. (**d**) Surface conservation plot of AAA2 and the linker cleft, color-coded as in **a**. Conserved surface patches are indicated by black dotted lines. The surface patch of AAA2 consists of two β-hairpins. (**e**) Color-coded cartoon representation of the plot shown in **d**. The β-hairpins of AAA2 are highlighted in red. The black arrowheads in **d** and **e** point to the linker cleft.

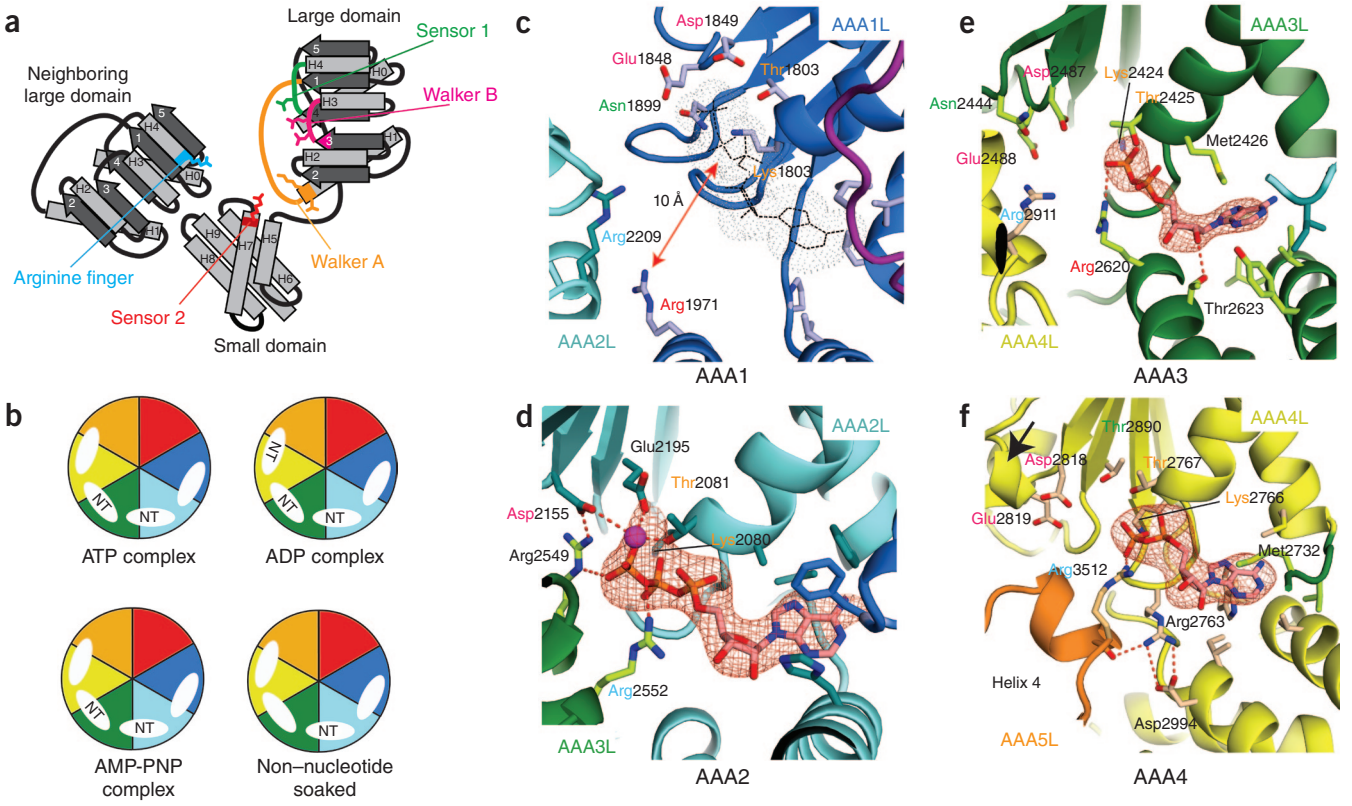

Figure 4 Nucleotide binding sites in the AAA+ ring. (**a**) Cartoon of an AAA+ nucleotide binding site showing essential residues (Walker A motif in orange, Walker B motif in pink, sensor 1 in green, sensor 2 in red and arginine finger in blue). (**b**) Schematic representation of the nucleotide binding states of the dynein motor domain for non–nucleotide soaked crystals (LuAc) and after soaking crystals with ADP, ATP or AMP-PNP. Color-coding is as in **Figure 1a**; NT, nucleotide. (**c**) AAA1 site showing how crucial nucleotide binding residues are moved away from the putative nucleotide position (gray) (ATP-soaked crystal structure). (**d**) AAA2 site showing density for a firmly bound Mg-ATP molecule mediating multiple interactions between AAA2 and AAA3 (unsoaked crystal structure). (**e**) AAA3 site showing density for an exchangeable ADP molecule (ADP-soaked crystal structure). (**f**) AAA4 site (ADP-soaked crystal structure). The catalytic Walker B glutamate is part of a short helical fragment (black arrow) and is angled away from the nucleotide. In all images, the $F_o - F_c$ difference density is contoured at 3σ, and hydrogen bond interactions are indicated by red dashed lines. In panels **c**–**f**, some residues of the nucleotide base binding pocket are shown in stick representation.

catalysis. The adenine base binding pocket is between the large and small domains, and further contacts to the ATP phosphate groups are made by conserved arginine residues on the small domain (sensor 2) and the neighboring large domain (arginine finger) (**Fig. 4a**). Work on other oligomeric AAA+ domains has shown that nucleotide binding closes the gap between the second and first large domain, either partially—typically in the presence of ADP—or completely, to bring the arginine finger into contact with the nucleotide[18–20].

In order to investigate nucleotide binding to the different AAA+ domains in dynein, we soaked crystals in ATP, ADP or AMP-PNP (**Fig. 4b**). Compared to the non–nucleotide soaked crystal structure, there are no major conformational changes. However, differences between the abilities of the nucleotides to bind individual AAA+ domains have emerged.

The AAA1 site (AAA1-AAA2 interface) is devoid of nucleotide in all of our structures (**Fig. 4b**), and the phosphate-binding Walker A P-loop on AAA1L is instead occupied by a sulfate ion (**Supplementary Fig. 4a**). The AAA1 site is in a very open conformation compared to the other nucleotide binding sites (**Supplementary Fig. 4a–d**). It is over 10-Å wide at the bottom and nearly 20-Å wide at the top. That nucleotide binding does not occur, even though all sites are accessible and AAA3 and AAA4 are occupied, demonstrates that the AAA1 site has a very low affinity for nucleotide in the conformation of dynein in our crystals. The reason for this low affinity is that the AAA1 small domain has swung down (**Supplementary Fig. 4e**,**f**) opening up the adenine base binding pocket so that the base would be more exposed to solvent than in the other nucleotide binding sites (**Supplementary Fig. 4g–h**). In addition, the small domain movement shifts the sensor 2 arginine residue so that it cannot contact the nucleotide phosphate groups (**Fig. 4c**).

The AAA2 site (AAA2-AAA3 interface) contains density for a Mg-ATP molecule even when crystals were not soaked in nucleotide, showing that it is tightly bound (**Fig. 4d** and **Supplementary Fig. 4b**). AAA2 lacks the catalytic glutamate in the Walker B motif. The position of this glutamate is occupied by a conserved arginine (Arg2549) from AAA3, which reaches over to contact the Walker B aspartate (Asp2155) and helps anchor the ATP in place (**Fig. 4d**). The nucleotide is also contacted by the arginine finger (Arg2552) from AAA3 and so adds to an extensive network of salt bridges and hydrophobic interactions that hold the AAA2 and AAA3 large domains together. Thus, the site is tightly closed and appears unlikely to open at any stage of the catalytic cycle.

The AAA3 nucleotide binding site (AAA3-AAA4 interface) contains all the nucleotide binding residues expected for an active AAA+ domain, arranged in the correct orientation (**Fig. 4e**). The AAA3 site is empty in the non–nucleotide soaked structure but is occupied in the presence of ATP, ADP and AMP-PNP (**Fig. 4b**). The nucleotide is more accessible than in the AAA2 site (61Å^2 of the nucleotide is solvent accessible compared to 44 Å^2 in the AAA2 site; see **Supplementary Fig. 4b**,**c**),

which is consistent with the AAA3 site having an intermediate nucleotide affinity. The adenine fits into the base binding pocket (**Supplementary Fig. 4h**) and packs against a methionine residue (Met2426), which moves in to make contact with it (**Fig. 4e**). The small domain of AAA3 makes contact with the nucleotide ribose from a conserved threonine residue (Thr2623) and with the nucleotide phosphate groups from the sensor arginine (Arg2620). The AAA3 site is in a semi-closed conformation (**Supplementary Fig. 4c**), similarly to other AAA+ proteins in their ADP state. The arginine finger from AAA4L (Arg2911) is still over 4.5 Å away from the nearest phosphate group, which suggests that the AAA3 site will close further in order for this residue to contact the nucleotide.

In the case of the AAA4 site (AAA4-AAA5 interface), only ADP soaks led to clear nucleotide binding (**Fig. 4b** and **Supplementary Fig. 4d**). The AAA4 site shows a number of unusual features in our structure. The proposed catalytic glutamate (Glu2819) is angled away from the nucleotide by the presence of a short α-helix (**Fig. 4f**), suggesting it is unable to catalyze ATP hydrolysis. The relative position of the two large domains is reminiscent of a fully closed nucleotide binding site, with the arginine finger (Arg3512) in position to contact the nucleotide. Despite the fact that the relative orientation of the large domains is similar to that of the AAA2 site, the nucleotide is not tightly buried (an 84-Å^2 area is solvent accessible; see **Supplementary Fig. 4d**). This is due to the exposure of the phosphate and ribose groups, as the base is buried to a similar extent as the nucleotide in AAA3 (**Supplementary Fig. 4h**,**i**). The positions of the large domains are stabilized in part by an arginine residue (Arg2763) located within the AAA4 Walker A P-loop, forming a hydrogen bond with helix 4 of AAA5L and a salt bridge with AAA4S (**Fig. 4f**).

DISCUSSION

During the dynein mechanochemical cycle, ATP binding and hydrolysis at AAA1 drives the linker into a pre–power stroke position close to AAA2 (refs. 5,11), whereas phosphate release allows return to the post–power stroke conformation. After the power stroke, ADP is released to reach the nucleotide-free (apo) state before ATP rebinding occurs[11]. Our structure was crystallized in the absence of nucleotide, and the linker is in a post–power stroke position, with its N terminus near the base of the stalk, suggesting it resembles the final, apo state of the dynein ATP cycle.

Both copies of the motor domain in the GST-dimerized construct are in a similar conformation (mean r.m.s. deviation is 1.3 Å), despite making different crystal packing contacts (**Supplementary Fig. 5a**,**b**), which indicates that crystallization doesn't distort the motor domain. Furthermore, the conserved nature of the AAA5 linker-binding site, together with our mutagenesis data, suggest that the post–power stroke state we observe is relevant to understanding the dynein ATPase cycle.

The low affinity of AAA1 for nucleotide in our structure is most likely due to the movement of the small domain, which both removes the sensor arginine and opens up the base binding pocket. The presence of low-affinity nucleotide binding sites is a known feature of AAA+ proteins, and it has been demonstrated structurally[20,21] and biochemically[22]. In the AAA+ family member ClpX, movement of the small domain is also responsible for the low-affinity nucleotide binding site, although in this case it is rotated in to sterically block access to the adenine binding pocket[20]. The large changes between low-affinity and nucleotide-bound states in AAA+ proteins are almost certainly incompatible with the crystalline state of the dynein motor domain, which explains why we could not observe nucleotide binding to AAA1 in our structure. Notably, crystals of the low-nucleotide affinity (rigor) conformation of myosin, a motor protein unrelated to the AAA+ family, can bind nucleotide when soaked with ADP[23]. However, in this case, the adenine base pocket is always fully established, so in contrast to the dynein AAA1 site, rigor myosin requires much smaller conformational changes for nucleotide binding.

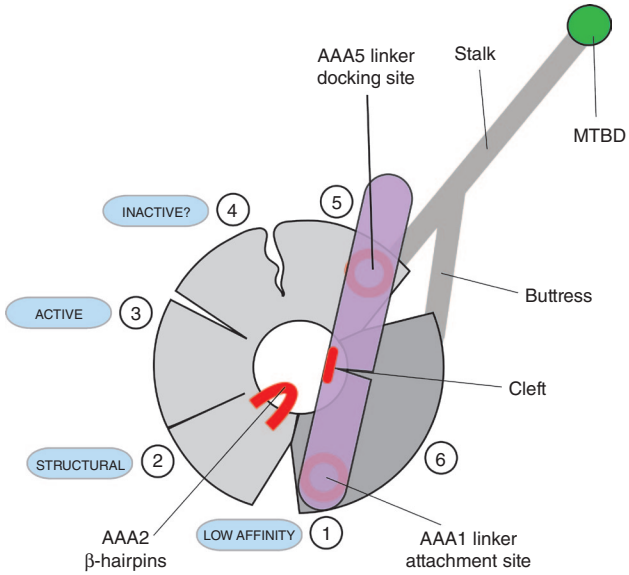

Figure 5 Schematic representation of the nucleotide-free dynein motor domain. The linker is in a post–power stroke position conformation and interacts with the AAA+ through conserved surface patches on AAA5 and AAA1. Conserved amino acid residues on the β-hairpins of AAA2 are in close proximity to a similarly conserved region near the linker cleft. A nucleotide-induced gap closure of the AAA1 site may bring these two areas into contact. The linker, in interacting with AAA5 and AAA1 at the same time, might act as a spacer pushing apart the two halves of the motor domain (light and dark gray) and causing a gap to open between AAA1-AAA2 and AAA5-AAA6. The gap at AAA1 leads to a low-nucleotide affinity state for this site. The AAA2 site contains a tightly bound ATP and is likely to have a purely structural role. Sites AAA3 and AAA4 appear to adopt a semi-closed conformation and can bind and release nucleotide. Although the AAA3 ATP hydrolysis site seems to be in a catalytically competent conformation, crucial catalytic residues of the AAA4 site might not be able to support ATP hydrolysis. The circled numbers indicate the location of AAA+ domains.

The recent low-resolution structure of a *Dictyostelium discoideum* dynein motor domain, crystallized in the presence of ADP (PDB 3AY1)[8], also has its linker in a post–power stroke conformation but with the N terminus of the linker closer to AAA4 and not making contact with the AAA5 site. A comparison of the *D. discoideum* and yeast structures suggests there are two different post–power stroke conformations of dynein. It is possible that the presence or absence of ADP is responsible for the differences in linker position or, in other words, that the interaction of the linker with AAA5 is associated with ejection of the nucleotide. Previous work did not consider the possibility of multiple post–power stroke conformations, but this may be because the difference in the linker positions is too small to be detected by the FRET[11,16,24] and negative-stain EM techniques that were used[6].

The gaps between AAA1L-AAA2L and AAA5L-AAA6L[7] appear to divide the AAA+ ring into two halves. We propose that the linker, when bound to AAA5L, acts as a spacer that pushes apart these two halves and opens up the AAA1 site to create a low-nucleotide affinity state. The result is an asymmetrical, non-planar overall conformation for the AAA+ ring. Consistent with this interpretation, the AAA+ ring in the *D. discoideum* crystal structure[8], where the linker does not contact AAA5L, shows a more symmetrical and planar arrangement of its building units. The effect of the AAA5L site mutations may thus be explained by a reduction in the ability of the motor domain to enter a low-affinity AAA1 site, so that the motor becomes trapped with nucleotide in its main hydrolysis site. Notably, the AAA5L site residues (Lys3438, Arg3445 and Phe3446) are very highly conserved only in cytoplasmic dyneins. In the IFT and inner-arm

axonemal dyneins, there is sequence similarity at these positions (**Fig. 3c**), suggesting they also use the AAA5 site for docking the linker to the ring. In the outer-arm dyneins, this site is not well conserved (**Fig. 3c**), so these motors may use a different strategy to release nucleotide from AAA1.

An important question is how the N terminus of the linker moves to its pre–power stroke state, exiting the ring near AAA2 (ref. 6). Our structure shows a conserved site on AAA2 that consists of a pair of β-hairpins. This site is adjacent to a conserved patch on the underside of the linker at the base of a hinge-like cleft. Modeling of the closed AAA1 conformation, based on the ATP-bound crystal structure of the AAA+ protein NtrC, suggests these two sites come into direct contact upon binding ATP (**Supplementary Fig. 5c–e**). We therefore propose that nucleotide binding detaches the linker from AAA5 and allows it to attach through a different site to AAA2. How this interaction results in the change in linker position observed by EM and whether it is causing the linker to bend at the hinge-like cleft are fascinating questions, but these will require further studies to elucidate.

Dyneins are unusual among motor proteins in having multiple nucleotide binding[10] sites. The mutagenesis of residues at AAA2, AAA3 and AAA4 leads to a decrease in velocity[12,13] but does not allow us to distinguish between structural, regulatory or catalytic roles. Our structure now builds on this work to provide further insight into the roles of these additional nucleotide binding sites. Our structure shows that the AAA3 site contains all the residues of an active AAA+ site, suggesting that it can hydrolyze ATP. However, these residues are not all conserved in axonemal and IFT dyneins. Furthermore, although mutagenesis of the Walker B catalytic glutamate impaired dynein velocity, it did not completely abrogate it, in contrast to the equivalent mutation at AAA1. The conformational changes in the AAA3 cleft must in some way contribute to the catalytic cycle, without being essential. The tightly bound nucleotide at AAA2 suggests it has a purely structural role and that mutations at this site act by disrupting the rigid AAA2-AAA3 interface and hence interfering with communication between AAA1 and AAA3.

In our structure, the AAA4 site appears to be in an inactive conformation. However, mutagenesis of the Walker A motif in AAA1 allows UV-mediated vanadate cleavage to occur at AAA4 (ref. 12), implying that the conformation of AAA4 may respond to events at AAA1. Therefore, we cannot rule out a conformational rearrangement that activates the AAA4 site at other points of dynein's catalytic cycle. It is notable, however, that the Walker B motif in AAA4 is not well conserved in IFT and axonemal dyneins, and mutation in cytoplasmic dyneins has no effect on velocity[13]. This suggests that whatever the role of AAA4, it is not required in all dyneins.

The main features of dynein revealed by our structure are summarized in **Figure 5**. In the absence of nucleotide, the linker spans the AAA+ ring contacting conserved patches at AAA5 and AAA1. The AAA1 site is wide open and has a low affinity for nucleotide. AAA2 binds nucleotide tightly and has a structural role. AAA3 appears active for ATP hydrolysis, whereas in this conformation, AAA4 does not. There is a cluster of conserved residues on AAA2 that is directly adjacent to a conserved patch on the underside of the linker at the base of a cleft. This may represent another interaction site with the linker. ATP binding to AAA1 would require closure of the gap between AAA1 and AAA2 and could bring these two conserved sites into proximity with each other.

METHODS

Methods and any associated references are available in the online version of the paper at http://www.nature.com/nsmb/.

Accession codes. The coordinates and structure factors for the ATP, ADP, AMP-PNP and LuAc complexes have been deposited in the Protein Data Bank with deposition codes 4AKG, 4AI6, 4AKH and 4AKI, respectively.

Note: Supplementary information is available on the Nature Structural & Molecular Biology website.

ACKNOWLEDGMENTS

We thank C. Cho for her work helping to identify heavy atom derivatives and suitable crystallization conditions. We also thank M. Schlager, A. Diamant, C. Cho, R. Vale, K. Nagai and L. Passmore for helpful discussions and their comments on the manuscript. This work was supported by the Medical Research Council (MC_UP_A025_1011 to A.P.C.).

AUTHOR CONTRIBUTIONS

E.S.G., H.S. and A.P.C. produced, purified and crystallized the protein. H.S. and E.S.G. prepared heavy atom derivatives. H.S. and A.P.C. collected data on crystals and determined the structure. H.S. carried out phasing. All authors built the model. E.S.G. and A.P.C. conducted the *in vitro* experiments. A.P.C. and H.S. wrote the paper.

COMPETING FINANCIAL INTERESTS

The authors declare no competing financial interests.

Published online at http://www.nature.com/nsmb/.
Reprints and permissions information is available online at http://www.nature.com/reprints/index.html.

1. Vallee, R.B., Williams, J.C., Varma, D. & Barnhart, L.E. Dynein: an ancient motor protein involved in multiple modes of transport. *J. Neurobiol.* **58**, 189–200 (2004).
2. Dodding, M.P. & Way, M. Coupling viruses to dynein and kinesin-1. *EMBO J.* **30**, 3527–3539 (2011).
3. Leigh, M.W. *et al.* Clinical and genetic aspects of primary ciliary dyskinesia/Kartagener syndrome. *Genet. Med.* **11**, 473–487 (2009).
4. Hafezparast, M. *et al.* Mutations in dynein link motor neuron degeneration to defects in retrograde transport. *Science* **300**, 808–812 (2003).
5. Burgess, S.A., Walker, M.L., Sakakibara, H., Knight, P.J. & Oiwa, K. Dynein structure and power stroke. *Nature* **421**, 715–718 (2003).
6. Roberts, A.J. *et al.* AAA+ Ring and linker swing mechanism in the dynein motor. *Cell* **136**, 485–495 (2009).
7. Carter, A.P., Cho, C., Jin, L. & Vale, R.D. Crystal structure of the dynein motor domain. *Science* **331**, 1159–1165 (2011).
8. Kon, T., Sutoh, K. & Kurisu, G. X-ray structure of a functional full-length dynein motor domain. *Nat. Struct. Mol. Biol.* **18**, 638–642 (2011).
9. Neuwald, A.F., Aravind, L., Spouge, J.L. & Koonin, E.V. AAA+: a class of chaperone-like ATPases associated with the assembly, operation, and disassembly of protein complexes. *Genome Res.* **9**, 27–43 (1999).
10. Gibbons, I.R., Gibbons, B.H., Mocz, G. & Asai, D.J. Multiple nucleotide-binding sites in the sequence of dynein beta heavy chain. *Nature* **352**, 640–643 (1991).
11. Kon, T., Mogami, T., Ohkura, R., Nishiura, M. & Sutoh, K. ATP hydrolysis cycle-dependent tail motions in cytoplasmic dynein. *Nat. Struct. Mol. Biol.* **12**, 513–519 (2005).
12. Kon, T., Nishiura, M., Ohkura, R., Toyoshima, Y.Y. & Sutoh, K. Distinct functions of nucleotide-binding/hydrolysis sites in the four AAA modules of cytoplasmic dynein. *Biochemistry* **43**, 11266–11274 (2004).
13. Cho, C., Reck-Peterson, S.L. & Vale, R.D. Regulatory ATPase sites of cytoplasmic dynein affect processivity and force generation. *J. Biol. Chem.* **283**, 25839–25845 (2008).
14. Reck-Peterson, S.L. *et al.* Single-molecule analysis of dynein processivity and stepping behavior. *Cell* **126**, 335–348 (2006).
15. Shimizu, T. & Johnson, K.A. Kinetic evidence for multiple dynein ATPase sites. *J. Biol. Chem.* **258**, 13841–13846 (1983).
16. Mogami, T., Kon, T., Ito, K. & Sutoh, K. Kinetic characterization of tail swing steps in the ATPase cycle of *Dictyostelium* cytoplasmic dynein. *J. Biol. Chem.* **282**, 21639–21644 (2007).
17. Ross, J.L., Wallace, K., Shuman, H., Goldman, Y.E. & Holzbaur, E.L. Processive bidirectional motion of dynein-dynactin complexes *in vitro*. *Nat. Cell Biol.* **8**, 562–570 (2006).
18. Chen, B. *et al.* Engagement of arginine finger to ATP triggers large conformational changes in NtrC1 AAA+ ATPase for remodeling bacterial RNA polymerase. *Structure* **18**, 1420–1430 (2010).
19. Davies, J.M., Brunger, A.T. & Weis, W.I. Improved structures of full-length p97, an AAA ATPase: implications for mechanisms of nucleotide-dependent conformational change. *Structure* **16**, 715–726 (2008).
20. Glynn, S.E., Martin, A., Nager, A.R., Baker, T.A. & Sauer, R.T. Structures of asymmetric ClpX hexamers reveal nucleotide-dependent motions in a AAA+ protein-unfolding machine. *Cell* **139**, 744–756 (2009).
21. Singleton, M.R., Sawaya, M.R., Ellenberger, T. & Wigley, D.B. Crystal structure of T7 gene 4 ring helicase indicates a mechanism for sequential hydrolysis of nucleotides. *Cell* **101**, 589–600 (2000).
22. Smith, D.M., Fraga, H., Reis, C., Kafri, G. & Goldberg, A.L. ATP binds to proteasomal ATPases in pairs with distinct functional effects, implying an ordered reaction cycle. *Cell* **144**, 526–538 (2011).
23. Coureux, P.D., Sweeney, H.L. & Houdusse, A. Three myosin V structures delineate essential features of chemo-mechanical transduction. *EMBO J.* **23**, 4527–4537 (2004).
24. Imamula, K., Kon, T., Ohkura, R. & Sutoh, K. The coordination of cyclic microtubule association/dissociation and tail swing of cytoplasmic dynein. *Proc. Natl. Acad. Sci. USA* **104**, 16134–16139 (2007).

ONLINE METHODS

Crystallization constructs. Crystals were produced with construct GST-Dyn1-314kD$_{\Delta 3039\text{-}3291}$, which is identical to the previously reported construct[7], that lacks the MTBD and has a truncated stalk region fused with the peptide PKAPPEEKEA. Crystals were also obtained with the construct GST-Dyn1-314kD$_{\Delta 3039\text{-}3289}$ that was produced by modifying GST-Dyn1-314kD$_{\Delta 3039\text{-}3291}$. The truncated stalk region in this case was fused with the peptide Gly-Asp. All genomic manipulations were carried out using standard molecular biology techniques.

Crystallization and data collection. Crystals of constructs GST-Dyn1-314kD$_{\Delta 3039\text{-}3291}$ or Dyn1-Dyn1-314kD$_{\Delta 3039\text{-}3289}$ were obtained by under-oil batch crystallization. A 3-µl aliquot of protein solution (6–15 mg ml^{-1} in 20 mM Tris-HCl 8.0, 100 mM KAc, 2 mM MgAc, 1 mM EGTA, 10% (v/v) glycerol and 1 mM DTT) was mixed with an equal amount of seeding solution produced from crystals that were resuspended in 12% (v/v) PEG3350, 100 mM sodium citrate, pH 5.7, and 200 mM ammonium sulfate and covered with 10 µl of Al's Oil (Hampton Research). The crystals for the seeding solution were produced with methods described previously[7]. Crystallization using the under-oil batch approach was carried out at 4 °C, and crystals grew to a maximal dimension of 0.8 × 0.4 × 0.2 mm^3. To obtain LuAc-derivatives, crystals were soaked overnight in solutions consisting of 5 mM LuAc, 100 mM Tris-HCl 7.5, 200 mM ammonium sulfate, 20% (v/v) PEG3350 and 15% (v/v) glycerol. We also tried to obtain LuAc-derivatives by co-crystallization trials in the presence of 1 mM LuAc, followed by quick soaking in cryoprotectant (100 mM sodium citrate, pH 5.7, 200 mM ammonium sulfate, 20% (v/v) PEG3350 and 15–20% (v/v) glycerol). However, in the later stages of data analysis, successful derivatization could not be detected, and we refer to this dataset as 'native'. WO_4-derivatization was carried out by transferring crystals into solutions containing 20 mM Na_2WO_4, 100 mM Tris-HCl 7.0, 200 mM ammonium sulfate, 20% (v/v) PEG3350 and 15% (v/v) glycerol for 4 h. The LuAc dataset originated from LuAc soaking experiments, and in terms of nucleotide binding we refer to this dataset as 'unsoaked' or 'non–nucleotide soaked'. The ADP-complex was produced by soaking crystals in 20 mM ADP, 100 mM sodium citrate, pH 5.7, 200 mM ammonium sulfate, 20% (v/v) PEG3350 and 20% (v/v) glycerol for 15 h. An alternative soaking condition also included 2 mM $MgCl_2$. However, both conditions produced similar results in terms of ligand binding. The ATP and AMP-PNP complexes were obtained by transferring crystals for 12 h into solutions consisting of 100 mM Tris-HCl 8.0, 200 mM ammonium sulfate, 20% (v/v) PEG3350, 20% (v/v) glycerol, 1 mM MgAc and 10 mM ATP or AMP-PNP, respectively. Using higher $MgCl_2$ and ATP concentrations (25 mM) in the soaking experiments did not substantially change the results in terms of ligand binding. The crystals used for the ADP and Na_2WO_4 soaking experiments were obtained with construct GST-Dyn1-314kD$_{\Delta 3039\text{-}3289}$; all other crystals were obtained with construct GST-Dyn1-314kD$_{\Delta 3039\text{-}3291}$. Crystals were directly plunge-frozen in liquid nitrogen before data collection. SAD data on the LuAc and Na_2WO_4 derivatives were collected at 100 K on beamline I02 at the Diamond Light source at a wavelength of 1.3408 Å or 1.21471 Å, respectively, and data collections on the nucleotide-soaked crystals were carried out at the European Synchrotron Radiation Facility or at the Diamond Light source. All datasets collected from single or multiple crystals were integrated and scaled using HKL2000 (ref. 25), XDS[26] or MOSFLM[27] and AIMLESS[28].

Structure determination. The location of heavy atom positions was determined from anomalous difference Fourier electron density maps calculated with FFT[29], using phases obtained by molecular replacement using PHASER[30], with the recently published low-resolution structure as a search model[7]. The derivative data along with the respective heavy atom positions were fed into the AutoSol wizard of PHENIX[31], using the SAD approach to produce experimentally phased electron density maps. The overall figures of merit after heavy atom phasing for the LuAc and Na_2WO_4 derivatives were 0.30 and 0.37, respectively. In addition, the native dataset was combined with previously obtained W12-cluster low-resolution phases[7]. The quality of electron density maps calculated from the native dataset was improved in combination with the derivative data using multicrystal averaging and phase extension in DMMULTI[32], which allowed for manual model building in Coot[33]. This preliminary model was used in a molecular-replacement approach for the dataset obtained from the ADP-soaked crystals, using PHASER[30]. The low-resolution data of the latter approach were incorporated in the multicrystal-averaging procedure described above to obtain an updated model. Further improvements were achieved by iterative rounds of refinement with REFMAC[34] or CNS[35] against the ADP-dataset, and manual rebuilding in Coot[33]. This final model was used as a search template in molecular replacement approaches with PHASER[30] against the datasets obtained from the ATP- and AMP-PNP–soaked crystals as well as from the LuAc derivative. The obtained models were updated by iterative rounds of refinement in REFMAC[34] and manual rebuilding in Coot[33]. The data and refinement statistics are summarized in **Table 1**. Figures were prepared using PYMOL (http://www.pymol.org). Alignments were carried out with CEALIGN[36], and surface area calculations were done with AREAIMOL[29] or SURFACE[29].

ATP-vanadate–mediated UV cleavage. A 10-µl portion of purified GST-Dyn1-314kD or GST-Dyn1-314kD$_{\Delta 3039\text{-}3291}$ (2–6 mg ml^{-1}) was diluted into 38 µL of buffer (50 mM HEPES, pH 7.5, 100 mM KAc, 5 mM MgAc, 1 mM DTT), followed by the addition of 1 µl of ATP-Mg (100 mM) and 1 µl of sodium orthovanadate (100 mM) solution. The sodium orthovanadate was incubated at 95 °C for 10 min before using. The samples were incubated on ice for 30 min then UV-irradiated for another 60 min and subsequently analyzed by SDS-PAGE.

Microtubule binding assay. Protein and microtubules were mixed and incubated with and without 10 mM ATP. The samples were centrifuged at 265,000*g* for 10 min. The supernatant was decanted, and the pellet was suspended in buffer (50 mM Tris-HCl, pH 8.0, 150 mM KAc, 2 mM MgAc, 1 mM EGTA, 10% (v/v) glycerol, 1 mM DTT and 10 µM taxol) to a volume equal to that of the supernatant. Input, supernatant and pellet samples were analyzed by SDS-PAGE.

Motility and ATPase assays. The motility and ATPase assays were carried out as described[14].

25. Otwinowski, Z. & Minor, W. Processing of X-ray diffraction data collected in oscillation mode. *Methods Enzymol.* **276**, 307–326 (1997).
26. Kabsch, W. Xds. *Acta Crystallogr. D Biol. Crystallogr.* **66**, 125–132 (2010).
27. Leslie, A.G.W. & Powell, H.R. Processing diffraction data with MOSFLM. in *Evolving Methods for Macromolecular Crystallography* Vol. 245 (eds. Read, R.J. & Sussman, J.L.) 41–51 (Springer, 2007).
28. Evans, P.R. An introduction to data reduction: space-group determination, scaling and intensity statistics. *Acta Crystallogr. D Biol. Crystallogr.* **67**, 282–292 (2011).
29. Collaborative Computational Project, Number 4. The CCP4 suite: programs for protein crystallography. *Acta Crystallogr. D Biol. Crystallogr.* **50**, 760–763 (1994).
30. McCoy, A.J. *et al.* Phaser crystallographic software. *J. Appl. Crystallogr.* **40**, 658–674 (2007).
31. Adams, P.D. *et al.* PHENIX: a comprehensive Python-based system for macromolecular structure solution. *Acta Crystallogr. D Biol. Crystallogr.* **66**, 213–221 (2010).
32. Cowtan, K. 'dm': an automated procedure for phase improvement by density modification. in *Joint CCP4 and ESF-EACBM Newsletter on Protein Crystallography* Vol. 31, 34–38. (Daresbury Laboratory, Warrington, UK, 1994).
33. Emsley, P. & Cowtan, K. Coot: model-building tools for molecular graphics. *Acta Crystallogr. D Biol. Crystallogr.* **60**, 2126–2132 (2004).
34. Murshudov, G.N., Vagin, A.A. & Dodson, E.J. Refinement of macromolecular structures by the maximum-likelihood method. *Acta Crystallogr. D Biol. Crystallogr.* **53**, 240–255 (1997).
35. Brünger, A.T. *et al.* Crystallography & NMR system: A new software suite for macromolecular structure determination. *Acta Crystallogr. D Biol. Crystallogr.* **54**, 905–921 (1998).
36. Shindyalov, I.N. & Bourne, P.E. Protein structure alignment by incremental combinatorial extension (CE) of the optimal path. *Protein Eng.* **11**, 739–747 (1998).

doi:10.1038/nsmb.2272